Journal of Magnetic Resonance **152,** 57-69 (2001)
doi:10.1006/jmre.2001.2377, available online at http://www.idealibrary.com on IDEAL®

Nonparametric NMR Spectroscopy[1]

Petre Stoica and Tomas Sundin

Department of Systems and Control, Uppsala University, P.O. Box 27, SE-75103 Uppsala, Sweden

E-mail: ps@syscon.uu.se; tsu@syscon.uu.se

Received December 12, 2000; revised April 16, 2001; published online August 1, 2001

The parametric (or model-based) approach to NMR spectroscopy suffers from two general problems: it is sensitive to modeling errors and requires knowledge of the number of resonances present in the compound(s) under analysis. The nonparametric approach has neither of these drawbacks and it may also be computationally simpler than the parametric approach. However, if not applied properly, the nonparametric approach may yield significantly less accurate spectroscopic results than the parametric approach. In this paper we introduce a high-resolution nonparametric methodology for NMR spectroscopy based on the adaptive filter bank approach. The main salient feature of the new approach is that it provides 2D spectra versus both frequency and damping, as opposed to the classical 1D frequency spectra routinely used in NMR spectroscopy. To show the power of our new nonparametric approach we compare its performance with the ultimate performance of the parametric approach. We use both simulated and real NMR signals in our numerical performance study. © 2001 Academic Press

Key Words: **magnetic resonance spectroscopy (MRS); nonparametric methods; adaptive filter bank methods; two-dimensional processing.**

1. INTRODUCTION AND PRELIMINARIES

The NMR signal is often modeled as a sum of damped sinusoids:

$$x(t) = \sum_{k=1}^{n} a_k e^{(-\alpha_k + i\omega_k)t} + \epsilon(t), \quad t = 1, 2, \ldots. \qquad [1]$$

In [1] n denotes the number of components (or resonances) deemed to be present in the compound(s) under analysis; $\{a_k \in \mathbb{C}\}$, $\{\alpha_k > 0\}$, and $\{\omega_k \in (0, 2\pi]\}$ are the amplitudes, damping factors, and (angular) frequencies of these components; and $\epsilon(t)$ is a noise term that includes both measurement and modeling errors. Note that the sampling interval corresponding to the discrete time data in [1] was absorbed in $\{\alpha_k\}$ and $\{\omega_k\}$ to simplify the notation. In some cases there is a priori information about some parameters in [1] (see, e.g., (1–4)). In other applications all parameters in [1] (including n) are unknown and must be estimated from the observed data $\{x(t)\}_{t=1,\ldots,N}$ (see, e.g., (5–7)); hereafter N denotes the number of available observations. In this paper we will focus on the latter case.

The nonlinear least-squares (NLS) method is one of the best *parametric* approaches that can be used to estimate the unknown parameters in [1]. The NLS estimates are given by the minimizing arguments of the following loss function:

$$\{\hat{a}_k, \hat{\alpha}_k, \hat{\omega}_k\} = \arg \min_{\{a_k, \alpha_k, \omega_k\}} \sum_{t=1}^{N} \left| x(t) - \sum_{k=1}^{n} a_k e^{(-\alpha_k + i\omega_k)t} \right|^2. \qquad [2]$$

When the noise $\epsilon(t)$ in [1] is white, circular, and Gaussian the NLS is asymptotically statistically efficient (see, e.g., (*1, 2*) and the references therein). If the noise does not satisfy the previous conditions, the NLS loses its statistical efficiency but it retains an appealing robustness usually associated with the LS fitting approaches; in effect, the NLS is one of the most robust parametric approaches to deviations from the white Gaussian noise assumption. On the negative side, the NLS requires the use of a nonlinear search algorithm over a $2n$-dimensional parameter space (the minimizer of [2] with respect to $\{a_k\}$ can be obtained in closed form and hence the dimension of the parameter space for the problem in [2] can be reduced from $4n$ to $2n$). Additionally, like any other parametric method, the NLS requires knowledge of n. In the performance study reported under Numerical Examples we compare the new *nonparametric* approach introduced in this paper with the best possible performance of the parametric methods (including the NLS) given by the Cramér–Rao lower bound (CRB) (*8*).

The Fourier transform (FT) method is the most commonly used *nonparametric* approach for spectroscopic analysis. Its main step consists of computing the FT complex spectrum

$$X(\omega) = \frac{1}{N} \sum_{t=1}^{N} x(t) e^{-i\omega t} \qquad [3]$$

[1] This work partly supported by the Senior Individual Grant Program of the Swedish Foundation for Strategic Research (SSF).

1090-7807/01 $35.00
Copyright © 2001 by Academic Press
All rights of reproduction in any form reserved.

for $\omega \in (0, 2\pi]$. After appropriate phase correction the locations of the dominant peaks of $\mathrm{Re}[X(\omega)]$ are the frequency estimates $\{\hat{\omega}_k\}$ and the area under the peaks are the amplitude estimates $\{\hat{a}_k\}$. The estimated spectrum in [3] can be conveniently evaluated using an FFT algorithm. However, the FT suffers from a number of well-known problems:

(a) $\mathrm{Re}[X(\omega)]$ is an erratic function of ω, which may hamper the selection of the right peaks corresponding to the frequencies ω_k in the observed data (this is particularly true at low SNR). With this observation in mind the fact that the FT requires no a priori knowledge about n is no longer a real advantage.

(b) the FT spectrum has poor resolution (two components in [1] that are closely spaced in frequency may appear as only a single peak in $\mathrm{Re}[X(\omega)]$), and it is adversely affected by leakage effects (for instance, the area under a peak at frequency ω_1 may be a rather poor estimate of a_1 owing to leakage from a stronger component at a frequency different from ω_1).

Problem (b) above is exacerbated for NMR signals. For such signals the overlapping between the true spectral peaks, owing to nonzero damping factors, may worsen the already poor resolution of the FT. Moreover, leakage from the water peak in ^{1}H spectroscopy, if not carefully eliminated by data preprocessing, may have a detrimental effect on the estimation accuracy for the other spectral peaks. Additionally, note that the FT does not provide any direct estimate of either the amplitudes $\{a_k\}$ or the damping factors $\{\alpha_k\}$.

One reason for all these drawbacks of the FT is that this approach yields 1D frequency spectra and hence ignores the information that the (noise-free) data consist of damped sinusoids, as opposed to pure sinusoids. A first step toward mitigating the problems of the classical FT is to introduce a 2D FT approach that is based on 2D spectra versus both frequency *and* damping. In the next section we derive the 2D FT in the general framework of the *filter bank approach* (FBA). As we explain there the 2D FT does not eliminate completely the problems of the 1D FT due to the fact that the filter bank corresponding to the 2D FT is still *nonadaptive* (i.e., data independent). To fully eliminate the aforementioned problems we need to take a second step and use an *adaptive* (i.e., data dependent) filter bank approach. Two most well-known adaptive FBA methods for 1D frequency spectrum estimation are:

- CAPON (*8, 9*) (named after the author of (*9*) who introduced it); and
- APES (*10, 11*) (APES is an acronym for *a*mplitude and *p*hase *e*stimation).

Similarly to the 1D FT, both CAPON and APES could be applied directly to the NMR signal to obtain estimates of $\{\omega_k\}$, but this would *not* be advisable since the information that the signal comprises damped sinusoids would again be ignored (in particular, no direct estimates of $\{a_k\}$ or $\{\alpha_k\}$ could be obtained in this way, as explained above for the 1D FT). *In this paper we develop new extensions of the CAPON and APES approaches that are suitable for damped sinusoidal signals in noise* (the versions of CAPON and APES previously proposed in the literature assume purely (undamped) sinusoidal signals and, as we already said, they are not really suitable for NMR signals). The so-obtained 2D CAPON and 2D APES are *nonparametric* FB approaches that do not suffer from any of the aforementioned problems of the FT. In particular, these methods possess the following desirable properties:

(i) their estimated spectra are relatively smooth, which makes it easy to choose the right peaks corresponding to the true $\{\alpha_k, \omega_k\}$ even at low SNR;

(ii) the resolution of these methods is excellent (by their 2D nature they can resolve peaks that overlap to a large extent in the 1D frequency spectrum);

(iii) owing to their adaptive nature these methods are almost leakage-free (they can even be applied in the presence of the water signal); and

(iv) they provide estimates not only of $\{\omega_k\}$ but also of $\{a_k\}$ and $\{\alpha_k\}$; moreover, the accuracy of these estimates is comparable with that corresponding to a good parametric approach (such as the NLS outlined above), under the ideal condition that the data model in [1] holds (required by the parametric approach).

When we add to the above features the robustness of the nonparametric methods to mismodeling and reiterate the fact that these methods do not require any a priori information about n, it becomes quite clear that the novel nonparametric approach of this paper is a valid alternative to the parametric approach for NMR spectroscopy.

2. THE 2D FILTER BANK APPROACH

Let

$$y(t) = [x(t) \cdots x(t + M - 1)]^T, \quad t = 1, 2, \ldots, L, \qquad [4]$$

where $M > 1$ is a user parameter (the choice of which will be discussed under Numerical Examples), and

$$L = N - M + 1. \qquad [5]$$

Also, let $h(\alpha, \omega) \in \mathbb{C}^{M \times 1}$ denote the coefficient vector of an FIR filter (to be applied to $\{x(t)\}$) which is such that:

(C1) the damped sinusoid $\{ae^{(-\alpha+i\omega)t}\}$ passes undistorted through the filter; and

(C2) other components in the data $\{x(t)\}$ (for example, the noise and other damped sinusoids) are suppressed as much as possible by the filter.

Note that such a filter must depend on α and ω, a fact which was indicated above by the use of the notation $h(\alpha, \omega)$. Also note that as α and ω vary $\{h(\alpha, \omega)\}$ will form a *bank of filters*, which gives the name of FBA to the approach based on $\{h(\alpha, \omega)\}$. Assuming that $h(\alpha, \omega)$ is available we can write the filter output

as

$$h^*(\alpha,\omega)y(t) = ae^{(-\alpha+i\omega)t} + w(t), \quad t = 1, 2, \ldots, L, \qquad [6]$$

where the superscript $*$ denotes the conjugate transpose, and $w(t)$ is a residual term. The LS estimate of the amplitude a in [6] is (for given α and ω)

$$\hat{a}(\alpha,\omega) = h^*(\alpha,\omega)Y(\alpha,\omega), \qquad [7]$$

where

$$Y(\alpha,\omega) = \frac{1}{L(\alpha)}\sum_{t=1}^{L}[y(t)e^{-\alpha t}]e^{-i\omega t} \qquad [8]$$

and where

$$L(\alpha) = \sum_{t=1}^{L} e^{-2\alpha t} = e^{-2\alpha}\frac{e^{-2\alpha L}-1}{e^{-2\alpha}-1}. \qquad [9]$$

Note that the numerator in [8] can be evaluated as a function of ω, for each value of α considered, by using an FFT algorithm. Let

$$E(\alpha,\omega) \triangleq |\hat{a}(\alpha,\omega)|^2 L(\alpha) \qquad [10]$$

denote the FBA 2D (estimated) *energy spectrum*. The FBA estimates $\{\hat{\alpha}_k, \hat{\omega}_k\}$ are obtained as the locations of the dominant peaks of $E(\alpha,\omega)$ (note that n is also estimated in the process of peak picking) and the estimates of $\{a_k\}$ are given by $\{\hat{a}_k = \hat{a}(\hat{\alpha}_k, \hat{\omega}_k)\}$.

Remark 1. We might think of using the estimated *amplitude spectrum* $A(\alpha,\omega) \triangleq |\hat{a}(\alpha,\omega)|$ to obtain the estimates $\{\hat{\alpha}_k, \hat{\omega}_k\}$. Under Numerical examples this possibility is examined and the results show that the energy and amplitude spectrum-based methods give similar results. However, the estimates obtained using the amplitude spectrum are slightly worse for low SNR cases and therefore the energy spectrum was preferred (see, e.g., Fig. 7 and Fig. 8).

Remark 2. As already stated $\hat{a}(\alpha,\omega)$ in [7] is the minimizer of the LS criterion:

$$\sum_{t=1}^{L}\left|h^*(\alpha,\omega)y(t) - ae^{(-\alpha+i\omega)t}\right|^2. \qquad [11]$$

Then we might think of inserting $\hat{a}(\alpha,\omega)$ in [11] and estimate the corresponding pair (α,ω) by minimizing the resulting LS criterion,

$$\begin{aligned}\sum_{t=1}^{L}\left|h^*(\alpha,\omega)y(t) - \hat{a}(\alpha,\omega)e^{(-\alpha+i\omega)t}\right|^2 &= \sum_{t=1}^{L}|h^*(\alpha,\omega)y(t)|^2 - |\hat{a}(\alpha,\omega)|^2 L(\alpha) \\ &= \sum_{t=1}^{L}|h^*(\alpha,\omega)y(t)|^2 - E(\alpha,\omega). \qquad [12]\end{aligned}$$

However, we do *not* recommend this way of estimating $\{\alpha_k, \omega_k\}$. A general reason for this (not necessarily related to NMR applications) can be explained as follows. Let us assume, for the sake of making our point, that for some given $(\bar{\alpha}, \bar{\omega})$ the left-hand side of [6] is very small: $h^*(\bar{\alpha}, \bar{\omega})y(t) \approx 0$ (for $t = 1, \ldots, L$). This means that there is hardly any damped sinusoid in the data at this particular damping-frequency pair $(\bar{\alpha}, \bar{\omega})$. A consequence of this is that the LS criterion in [12] will take on a very small value at $(\bar{\alpha}, \bar{\omega})$, and hence this pair may well be preferred to a true damping-frequency pair at which the criterion [12] may have a larger value.

In summary, estimating $\{\alpha_k, \omega_k\}$ by picking the dominant peaks of the energy spectrum $E(\alpha,\omega)$ is a more sensible thing to do than picking the deepest valleys of the criterion in [12].

Next we turn our attention to the conditions C1 and C2 above that must be satisfied by $h(\alpha,\omega)$. Satisfying C1 is easy. Let

$$s(\alpha,\omega) = \left[1\; e^{-\alpha+i\omega} \cdots e^{(-\alpha+i\omega)(M-1)}\right]^T. \qquad [13]$$

When the filter $h(\alpha,\omega)$ is fed with $ae^{(-\alpha+i\omega)t}$ its output is given by

$$[h^*(\alpha,\omega)s(\alpha,\omega)]ae^{(-\alpha+i\omega)t}. \qquad [14]$$

It follows that C1 is satisfied if and only if

$$h^*(\alpha,\omega)s(\alpha,\omega) = 1. \qquad [15]$$

Unlike C1, there is no unique way to formulate C2 mathematically. In the next subsections we show how different ways of formulating C2 lead to different FBA methods. Here we note that the importance of C2 cannot be emphasized enough. If the filter significantly enhances the currently considered damped sinusoid at (α,ω), then the SNR for this component in the filter output [6] will be much higher than in the raw data. Consequently, the estimation of $\{a_k, \alpha_k, \omega_k\}$ may well be done more accurately from the filtered data than from the raw data, despite a loss in the number of data samples (there are $M-1$ more data samples in the raw data).[2] This is the *basic idea* underlying the FBA.

[2] Observe that, owing to the manner in which we implemented the filtering (see [4]–[5]), we lose samples from the tail of the data string. As the SNR of those samples is typically rather low, this is not a big loss.

2.1. 2D FT

The 2D FT corresponds to the choice

$$h_{FT}(\alpha, \omega) = \frac{s(\alpha, \omega)}{\|s(\alpha, \omega)\|^2}, \quad [16]$$

where

$$\|s(\alpha, \omega)\|^2 = \frac{e^{-2\alpha M} - 1}{e^{-2\alpha} - 1}. \quad [17]$$

Obviously [16] satisfies the condition C1 in [15]. However, the above filter $h_{FT}(\alpha, \omega)$ does not have good rejection properties (see C2). In particular, note that [16] is nonadaptive and hence a strong component with damping and frequency different from (α, ω) may well leak through the filter and seriously disturb the estimation of the amplitude at (α, ω). To alleviate this leakage problem we should consider *adaptive* filters, as described in the next subsections. To end this subsection we remark on the fact that for $M = 1$ the present approach reduces to the "nonaveraged" (or "nonsmoothed") 2D FT,

$$\hat{a}(\alpha, \omega) = \frac{\sum_{t=1}^{N} [x(t)e^{-\alpha t}]e^{-i\omega t}}{\sum_{t=1}^{N} e^{-2\alpha t}}, \quad [18]$$

which, in turn, reduces for $\alpha = 0$ to the classical 1D FT in [3].

2.2. 2D CAPON

The filter bank associated with the 2D CAPON method is the solution to the following design problem,

$$\min_{h(\alpha,\omega)} \sum_{t=1}^{L} |h^*(\alpha, \omega)y(t)|^2 \quad [19]$$

subject to the condition C1,

$$h^*(\alpha, \omega)s(\alpha, \omega) = 1. \quad [20]$$

The criterion in [19] can be rewritten as

$$\sum_{t=1}^{L} |h^*(\alpha, \omega)y(t)|^2 = h^*(\alpha, \omega)Rh(\alpha, \omega), \quad [21]$$

where

$$R = \sum_{t=1}^{L} y(t)y^*(t). \quad [22]$$

Minimization of the sample energy of the filter output as in [19], under C1, should yield a filter with good rejection/enhancing properties. The solution to the linearly constrained quadratic problem in [19] and [20] is given by (see, e.g., (*8, 9*))

$$h_{CAPON}(\alpha, \omega) = \frac{R^{-1}s(\alpha, \omega)}{s^*(\alpha, \omega)R^{-1}s(\alpha, \omega)}. \quad [23]$$

Note that

$$s(\alpha, \omega) = \begin{bmatrix} 1 & & 0 \\ & e^{-\alpha} & \\ & & \ddots \\ 0 & & e^{-\alpha(M-1)} \end{bmatrix} \begin{bmatrix} 1 \\ e^{i\omega} \\ \vdots \\ e^{i\omega(M-1)} \end{bmatrix}, \quad [24]$$

where $[1\, e^{i\omega} \cdots e^{i\omega(M-1)}]^T$ is the 1D FT vector. Hence, for any given α, we can redefine R^{-1} appropriately and compute $h_{CAPON}(\alpha, \omega)$ and the corresponding $\hat{a}(\alpha, \omega)$ in [7] as functions of ω by using the fast 1D CAPON algorithm in (*12*).

2.3. 2D APES

In the 2D APES approach C2 is formulated in words as follows: $h(\alpha, \omega)$ should be such that the filter output $h^*(\alpha, \omega)y(t)$ is as close as possible in the LS sense to a damped sinusoid $ae^{(-\alpha+i\omega)t}$ with the given damping and frequency (α, ω) and amplitude a that minimizes the LS fitting error. Mathematically, for given α and ω, we obtain $h_{APES}(\alpha, \omega)$ and $\hat{a}_{APES}(\alpha, \omega)$ by minimizing the LS criterion,

$$\sum_{t=1}^{L} \left|h^*(\alpha, \omega)y(t) - ae^{(-\alpha+i\omega)t}\right|^2 \quad [25]$$

subject to the condition C1 (see [20]). The 2D APES estimate of $a(\alpha, \omega)$ is readily seen to have the form of the general FBA estimate in [7]. Inserting [7] in the criterion function yields

$$\begin{aligned} &\sum_{t=1}^{L} \left|h^*(\alpha, \omega)\left[y(t) - Y(\alpha, \omega)e^{(-\alpha+i\omega)t}\right]\right|^2 \\ &\quad = h^*(\alpha, \omega)[R - 2L(\alpha)Y(\alpha, \omega)Y^*(\alpha, \omega) \\ &\qquad + L(\alpha)Y(\alpha, \omega)Y^*(\alpha, \omega)]h(\alpha, \omega) \\ &\quad = h^*(\alpha, \omega)Q(\alpha, \omega)h(\alpha, \omega), \end{aligned} \quad [26]$$

where

$$Q(\alpha, \omega) = R - L(\alpha)Y(\alpha, \omega)Y^*(\alpha, \omega). \quad [27]$$

It follows that $h_{APES}(\alpha, \omega)$ is the solution to the following optimization problem,

$$\begin{aligned} &\min_{h(\alpha,\omega)} h^*(\alpha, \omega)Q(\alpha, \omega)h(\alpha, \omega) \\ &\text{subject to } h^*(\alpha, \omega)s(\alpha, \omega) = 1, \end{aligned} \quad [28]$$

which has same form as the CAPON filter design problem (with the only difference that R in [21] is replaced by $Q(\alpha, \omega)$ here). Hence, the solution to [28] is similarly to [23] given by

$$h_{APES} = \frac{Q^{-1}(\alpha, \omega)s(\alpha, \omega)}{s^*(\alpha, \omega)Q^{-1}(\alpha, \omega)s(\alpha, \omega)}. \quad [29]$$

To avoid the calculation of the inverse in [29] for every pair (α, ω) considered, we use the matrix inversion lemma (see, e.g., (*8*)) to write

$$Q^{-1}(\alpha, \omega) = R^{-1} + \frac{R^{-1}L(\alpha)Y(\alpha, \omega)Y^*(\alpha, \omega)R^{-1}}{1 - L(\alpha)Y^*(\alpha, \omega)R^{-1}Y(\alpha, \omega)}. \quad [30]$$

Combining [29] and [30] gives a formula for the 2D APES filter bank that is not much more computationally involved than the formula in [30] corresponding to the 2D CAPON.

2.4. 2D CAPES

There is empirical evidence (see, e.g., (*13*) for the undamped sinusoid case) which suggests that CAPON has a (slightly) higher resolution than APES and also that the CAPON estimates of the $\{\alpha_k, \omega_k\}$ are more accurate than the APES estimates of these parameters. On the other hand, for a given set of estimates $\{\hat{\alpha}_k, \hat{\omega}_k\}$ in the vicinity of the true values $\{\alpha_k, \omega_k\}$, the APES estimates of the amplitudes $\{a_k\}$ are (much) more accurate than the CAPON estimates of $\{a_k\}$. Consequently, the nonparametric approach we propose for NMR spectroscopy consists of the following combination of 2D CAPON and 2D APES, which we call 2D CAPES.

Nonparametric NMR Spectroscopy via 2D CAPES

Step 1. Obtain estimates of $\{\alpha_k, \omega_k\}$ as the locations of the dominant peaks of the 2D CAPON energy spectrum $|h^*_{CAPON}(\alpha, \omega)Y(\alpha, \omega)|^2 L(\alpha)$ with $h_{CAPON}(\alpha, \omega)$ given by [23] and $Y(\alpha, \omega)$ by [8] and [9]. Note that the required peak picking, at the level of SNR encountered in NMR applications, is usually easily done (see the illustrations under Numerical Examples).

Step 2. Estimate the amplitudes $\{a_k\}$ as $\hat{a}_k = h^*_{APES}(\hat{\alpha}_k, \hat{\omega}_k)$ $Y(\hat{\alpha}_k, \hat{\omega}_k)$, where $\{\hat{\alpha}_k, \hat{\omega}_k\}$ are the estimates of $\{\alpha_k, \omega_k\}$ obtained in Step 1, and $h_{APES}(\alpha, \omega)$ is given by [29] and [30].

The computational burden of 2D CAPES is similar to that of 2D CAPON and hence smaller than that of the 2D APES. Even so, as already stated, the statistical performance of 2D CAPES is typically better than that of both 2D CAPON and 2D APES.

Compared with the 1D nonparametric approach (such as the 1D FT), the computational burden of our 2D CAPES is of course (much) larger. In fact to keep the computational burden of 2D CAPES under a reasonable limit a careful implementation is required. *An efficient Matlab code for 2D CAPES is available from the authors on request.*

3. NUMERICAL EXAMPLES

In this section 2D CAPES is applied to both real NMR data and simulated data with the objective of examining its resolution properties and estimation accuracy.

Simulated Signal Examples

First the high resolution of the 2D CAPON energy spectrum is illustrated using a simulated two-peak example with the parameters (see the model in [1])

$$\begin{aligned} \omega_1 &= 0.1885, \quad \omega_2 = 0.2136 \\ \alpha_1 &= 0.0160, \quad \alpha_2 = 0.0260 \\ a_1 &= 1.0000, \quad a_2 = 2.5000 \\ N &= 512 \\ \sigma^2 &= 0.0010, \end{aligned} \quad [31]$$

where σ^2 denotes the variance of the white, circular, Gaussian noise sequence, $\epsilon(t)$. The real value of the 1D FT spectrum of the simulated signal is plotted in Fig. 1. From the figure it is clear that the two closely spaced peaks are not resolved by the 1D FT. It is possible to improve the resolution of the 1D FT by using a Lorenz-to-Gauss transformation of the time domain data:

$$x_G(t) = x(t)e^{\alpha_0 t - \beta_0 t^2}. \quad [32]$$

The best possible resolution is obtained if α_0 is set equal to the $\{\alpha_k\}$ of the peaks in the data. Since in general the $\{\alpha_k\}$ are not identical and they are also unknown, the choice of a suitable α_0 is not straightforward. In practice, the user has to tune the α_0 and

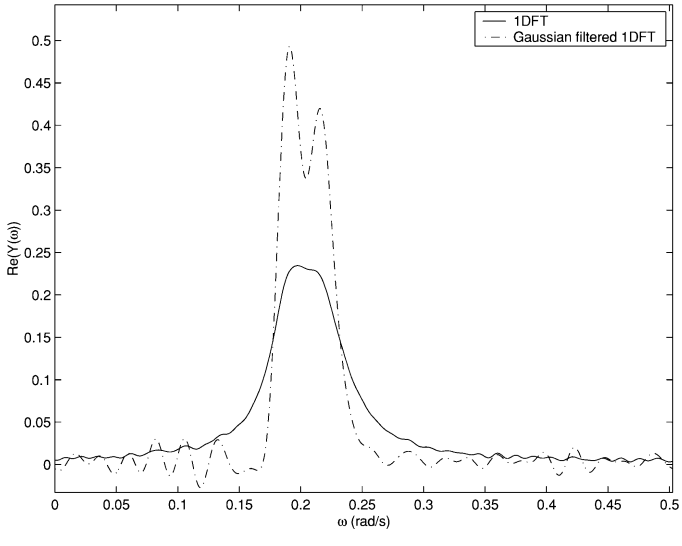

FIG. 1. Real value of the 1D FT spectrum for the simulated two-peak example: $a_1 = 1$, $a_2 = 2.5$, $\omega_1 = 0.1885$, $\omega_2 = 0.2136$, $\alpha_1 = 0.016$, $\alpha_2 = 0.026$, $N = 512$.

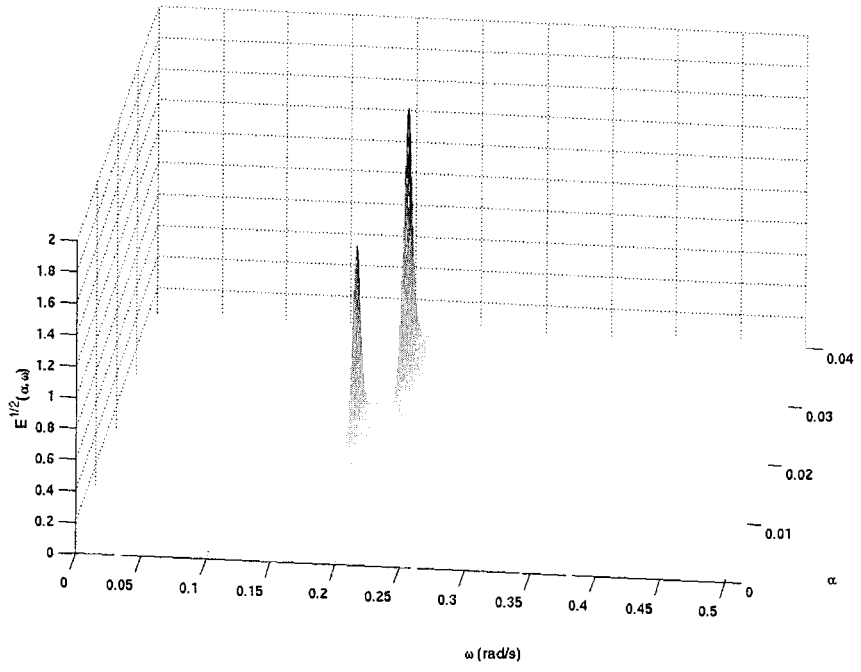

FIG. 2. 2D CAPON energy spectrum for the simulated two-peak example: $a_1 = 1$, $a_2 = 2.5$, $\omega_1 = 0.1885$, $\omega_2 = 0.2136$, $\alpha_1 = 0.016$, $\alpha_2 = 0.026$, $N = 512$, $M = 240$.

β_0 parameters by hand to obtain an enhanced resolution. In Fig. 1 the 1D FT of the so-called Gaussian-filtered data in [32] is also plotted. Note that the parameters were tuned to obtain the highest possible resolution resulting in a slight improvement over the 1D FT spectrum. In Fig. 2 the corresponding 2D CAPON energy spectrum using a filter length of $M = 240$ is plotted. The high resolution of 2D CAPON is illustrated by the ability to resolve the two peaks in *both* the frequency *and* the damping dimensions. To allow the reader to appreciate the resolution capabilities and to simplify the comparison of the peak locations with the true parameters the same 2D spectrum seen from above is plotted in Fig. 3. Finally the 2D CAPON spectrum viewed from the frequency axis (taking the maximum value of the energy in the damping dimension for each frequency grid point) can be found in Fig. 4. Note that this last plot does not contain all the information available in the 2D energy spectrum but can still be useful for comparison with the commonly used 1D FT spectrum in Fig. 1. In summary, this simple example shows that the resolution of the CAPON energy spectrum is much higher than that of the 1D FT even if the data are Gaussian filtered. The choice of the CAPON user parameter, M, is also much simpler than the choice of the parameters associated with the Gaussian filtering procedure in [32].

Next the influence of the user parameter M (i.e., the FIR filter length) on the estimation accuracy is examined. The choice of filter length is based on a trade-off between the resolution capabilities and the variance of the parameter estimates. To illustrate this trade-off the frequency separation, $\Delta\omega \stackrel{\triangle}{=} \omega_2 - \omega_1$, in the above two-peak example was varied. Estimates of the parameters of peak 1 were obtained from 100 independent simulation runs using different filter lengths, M. The variance of the noise was chosen so that the SNR for peak 1 was 15 dB where the SNR is defined as the ratio of the power of the component to the noise power:

$$\frac{1}{N}\sum_{t=1}^{N} |a_1|^2 e^{-2\alpha_1 t} \Big/ \sigma^2 \stackrel{\triangle}{=} \text{SNR}. \qquad [33]$$

The estimated root mean square error (RMSE) and bias of $\hat{a}_1$ and $\hat{\omega}_1$ are given in Fig. 5 and Fig. 6, respectively. The results for α_1 were similar to the results for a_1 and are therefore omitted. It can be seen that the bias of the estimates, as expected, decreases as a function of the filter length. At the same time the variance of the parameter estimates increases as a function of the filter length. However, since the variance increases relatively slowly compared to the decreasing bias, the RMSE error curves are reasonably flat for sufficiently high filter lengths (i.e., for M large enough to resolve the two peaks). It is in fact evident that the optimal filter length increases as the frequency separation between the peaks decreases. Therefore the choice of a relatively large M is recommended in general (in practice between $N/3$ and $N/2$). For difficult scenarios the filter length can be chosen close to the upper limit $N/2$.

Finally the estimation accuracy of the 2D CAPES method is compared to the CRB. Estimates of the parameters of peak 1 at $\omega_1 = 0.1885$ (for $\omega_2 = 0.2199$) were obtained from 100 independent simulation runs for different noise levels using a filter length of $M = 180$. The results for α_1 and a_1 are given in Fig. 7 and Fig. 8, respectively. Note that results obtained from both the amplitude spectrum and the energy spectrum are given, for

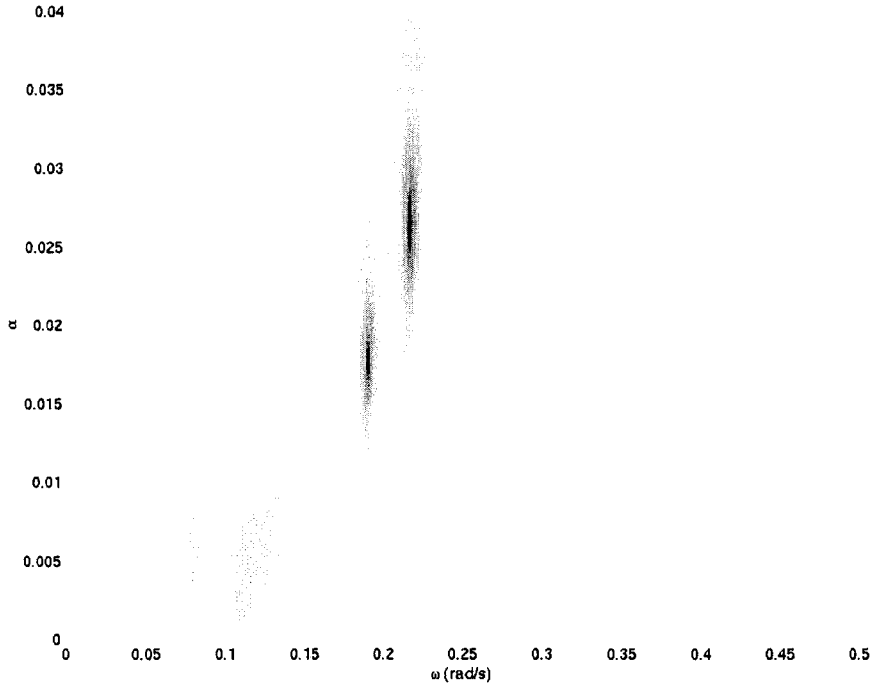

FIG. 3. Top view of the 2D CAPON energy spectrum for the simulated two-peak example: $a_1 = 1$, $a_2 = 2.5$, $\omega_1 = 0.1885$, $\omega_2 = 0.2136$, $\alpha_1 = 0.016$, $\alpha_2 = 0.026$, $N = 512$, $M = 240$.

comparative purposes. The figures indicate a slightly lower bias for estimates obtained by the energy spectrum, thereby suggesting that the energy spectrum should be the preferred choice (see Remark 1 under The 2D Filter Bank Approach). The parametric NLS method (e.g. (*1, 2*)) is expected (but not guaranteed) to have an accuracy close to the CRB under the above ideal simulation conditions (i.e., white, circular, and Gaussian noise and no modeling errors). The RMSE (based on the energy spectrum) of 2D CAPES is seen to be also reasonably close to the CRB.

Real NMR Signal Examples

In this section the resolution capability of the 2D CAPON energy spectrum is compared to that of the commonly used 1D FT

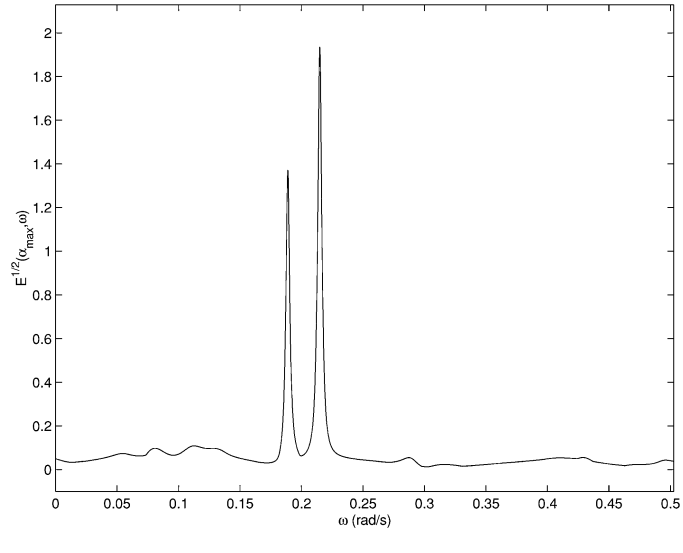

FIG. 4. 1D frequency view of the 2D CAPON energy spectrum for the simulated two-peak example: $a_1 = 1$, $a_2 = 2.5$, $\omega_1 = 0.1885$, $\omega_2 = 0.2136$, $\alpha_1 = 0.016$, $\alpha_2 = 0.026$, $N = 512$, $M = 240$.

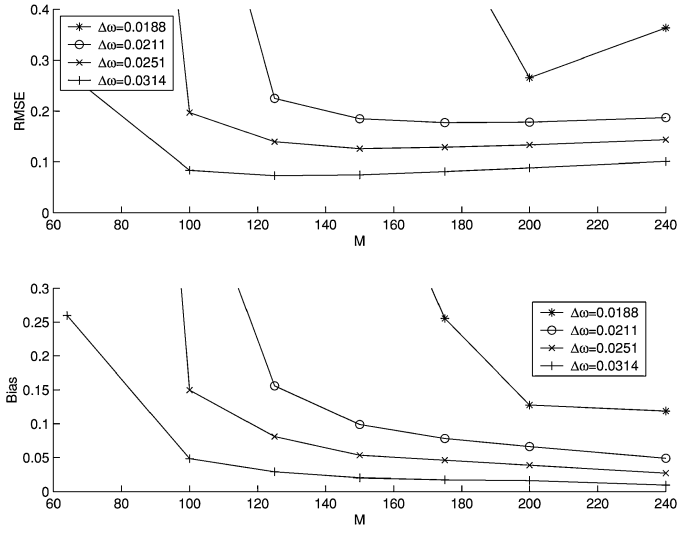

FIG. 5. RMSE and bias of 2D CAPES amplitude estimates as a function of filter length M for different frequency separations $\Delta\omega$ in a two-peak simulation example. The results were obtained from 100 simulation runs for each combination of M and $\Delta\omega$.

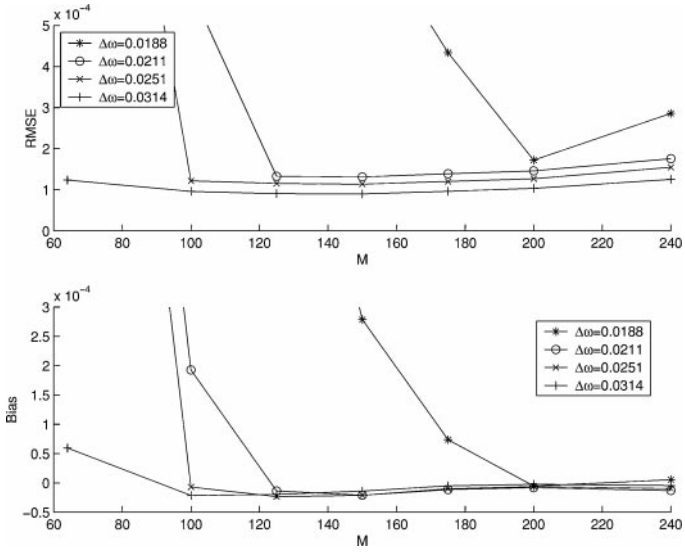

FIG. 6. RMSE and bias of 2D CAPES frequency estimates as a function of filter length M for different frequency separations $\Delta\omega$ in a two-peak simulation example. The results were obtained from 100 simulation runs for each combination of M and $\Delta\omega$.

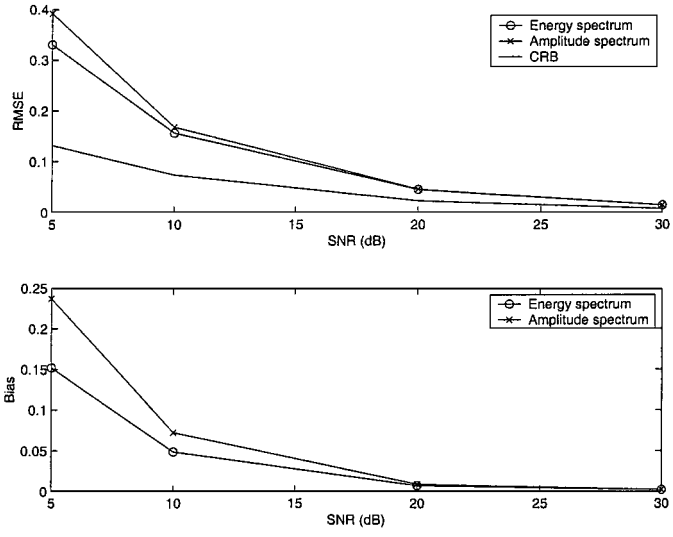

FIG. 8. RMSE and bias of 2D CAPES amplitude estimates ($M = 180$) as a function of SNR for the two-peak simulation example. The estimates were obtained from 100 simulation runs for each SNR level using both the energy spectrum and the amplitude spectrum. The RMSE is also compared to the CRB.

using real NMR data sets. Since the model and noise assumptions can no longer be expected to hold exactly, these examples provide a more realistic comparison between the methods. The first data set is taken from a standard GE spectroscopic phantom with a low-concentration additional GABA solution. The phantom contains 12.5 mM NAA, 10.0 mM Cr, 3.0 mM Ch, 7.5 mM mI, 12.5 mM Glu (L-glutamic acid), 5 mM *l*actate, and 0.5 mM GABA. Data were acquired on a 1.5-T GE Signa clinical MRI scanner equipped with 40 mT/m gradients at a 150 T/m/s slew rate. The single-voxel acquisition protocol on the scanner (*16*) implements a PRESS (*14*) excitation, preceded by CHESS (*15*) water suppression. Timing parameters were TE = 144 ms and TR = 1500 ms, and voxel size was 8 cc. Reference data (8 FIDs, two averages each) were acquired without water suppression, while the metabolite data were acquired with CHESS water suppression (32 FIDs, two averages each). The spectral bandwidth was 2500 Hz; $N = 2048$ points were sampled for each readout. The metabolite data were phase-corrected by subtracting the estimated phase obtained from the high-SNR reference signal (see, e.g., (*17*, *18*). In Fig. 9 the phase-corrected 1D FT spectrum for the region of interest is given where the peaks identified by numbers correspond to the following: 1, 5, *myo*-inositol; 2, 7, creatine; 3, 4, 12–15, glutamate; 6, choline, 8–11, 16, NAA; and 17, 18, lactate (the lactate peaks are negative for TE = 144 ms due to the coupled spin). Note that Gaussian filtering was applied to the data but since no significant resolution enhancement could be observed the corresponding 1D FT spectrum was not included. In Fig. 10 the 2D CAPON energy spectrum ($M = 950$) for the same signal is given. The resolution is much enhanced compared to the 1D FT spectrum. Note in particular the region between 2.1 and 2.8 ppm where the small-amplitude NAA and glutamate peaks are nicely resolved. It is also interesting to note that the 2D CAPON spectrum shows that the residual water peak consists of more than one damped sinusoid whereas the other peaks seem pretty well described by single damped sinusoids. That kind of information can not be deducted from the 1D FT spectrum. Furthermore this proves the robustness of our nonparametric approach as compared to parametric estimation methods which require the use of postprocessing water suppression techniques to handle the model imperfections of the

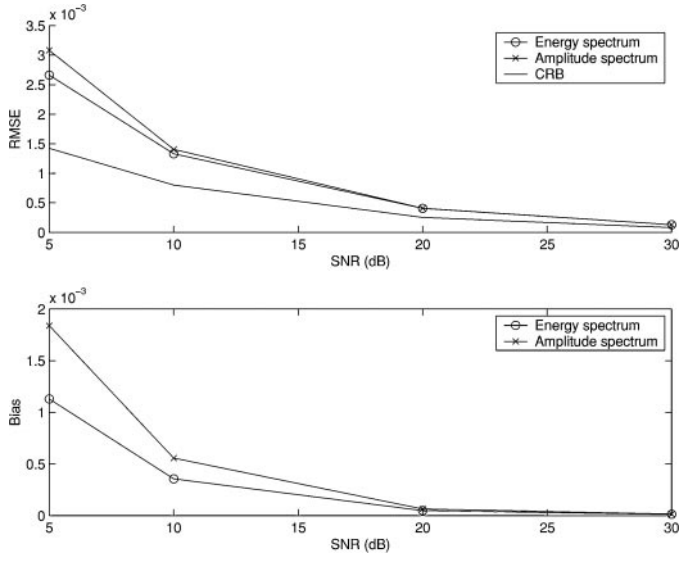

FIG. 7. RMSE and bias of 2D CAPES damping estimates ($M = 180$) as a function of SNR for the two-peak simulation example. The estimates were obtained from 100 simulation runs for each SNR level using both the energy spectrum and the amplitude spectrum. The RMSE is also compared to the CRB.

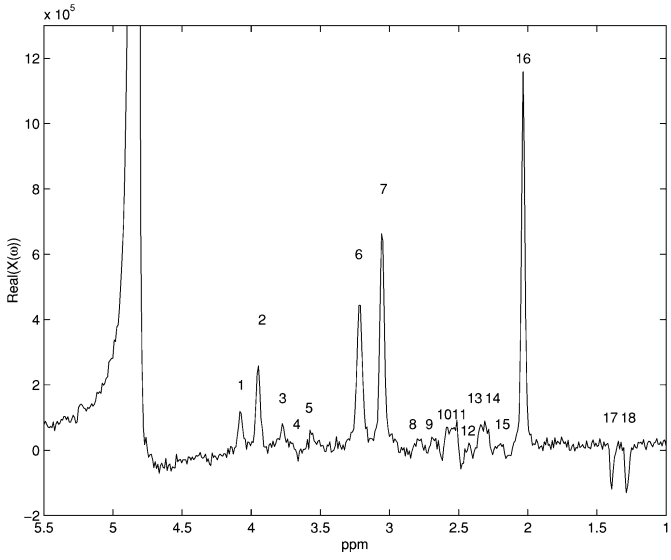

FIG. 9. Phase-corrected 1D FT spectrum obtained from a standard GE spectroscopic phantom. The phantom contains 12.5 mM NAA, 10.0 mM Cr, 3.0 mM Ch, 7.5 mM mI, 12.5 mM Glu (L-glutamic acid), 5 mM lactate, and 0.5 mM GABA. The signal was acquired on a 1.5-T GE Signa scanner using a PRESS sequence (TE/TR = 144/1500 ms) preceded by CHESS water suppression (voxel size 8 cc). The peaks identified by numbers correspond to the following: 1,5, *myo*-inositol; 2,7, creatine; 3,4, 12–15, glutamate; 6, choline; 8–11, 16, NAA; and 17,18, lactate.

residual water peak. The high resolution in both the frequency and damping domains can also be seen in Fig. 11 where the same 2D CAPON spectrum is plotted viewed from above. For completeness the 2D CAPON spectrum is also plotted as viewed from the frequency axis in Fig. 12. Even though the resolution cannot be fully appreciated using this 1D view the resemblance with the 1D FT spectrum in Fig. 9 gives some insight and may be useful to identify the peaks for spectroscopists more familiar with standard 1D FT spectra. We remind the reader that the height of the peaks in the 2D CAPON energy spectrum should not be considered direct estimates of the energies (or indirect amplitude estimates). In fact, when applying the 2D CAPES algorithm, only the frequency and damping estimates are obtained from the 2D CAPON energy spectrum. The amplitude estimates are instead obtained using the 2D APES algorithm (see Step 2 of the 2D CAPES algorithm in the previous section), and these estimates are usually significantly better. In Table 1 the CAPON and CAPES amplitude estimates are given for the dominant peaks 6, 7, and 16. The theoretical amplitude ratios of these peaks can be computed since the concentrations of the contents of the spectral phantom are known. Note that the data were acquired at TE = 144 ms; therefore, due to the different relaxation times of the metabolites, the actual amplitude ratios are different from the theoretical values. This makes an exact comparison of the estimated amplitude ratios rather difficult. The results, however,

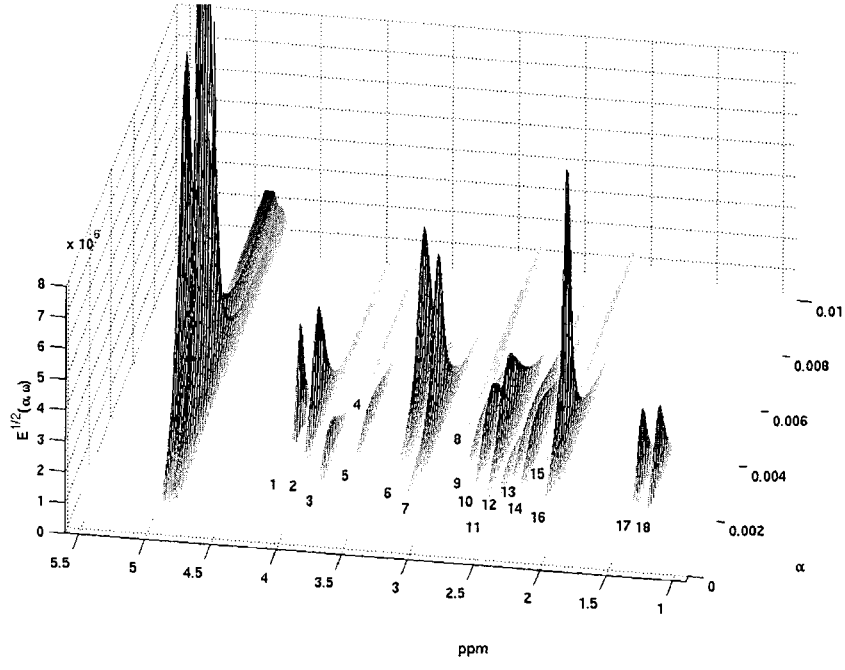

FIG. 10. 2D CAPON energy spectrum ($M = 950$) obtained from a standard GE spectroscopic phantom. The phantom contains 12.5 mM NAA, 10.0 mM Cr, 3.0 mM Ch, 7.5 mM mI, 12.5 mM Glu (L-glutamic acid), 5 mM lactate, and 0.5 mM GABA. The signal was acquired on a 1.5-T GE Signa scanner using a PRESS sequence (TE/TR = 144/1500 ms) preceded by CHESS water suppression (voxel size 8 cc). The peaks identified by numbers correspond to the following: 1,5, *myo*-inositol; 2,7, creatine; 3,4, 12–15, glutamate; 6, choline; 8–11, 16, NAA; and 17,18, lactate.

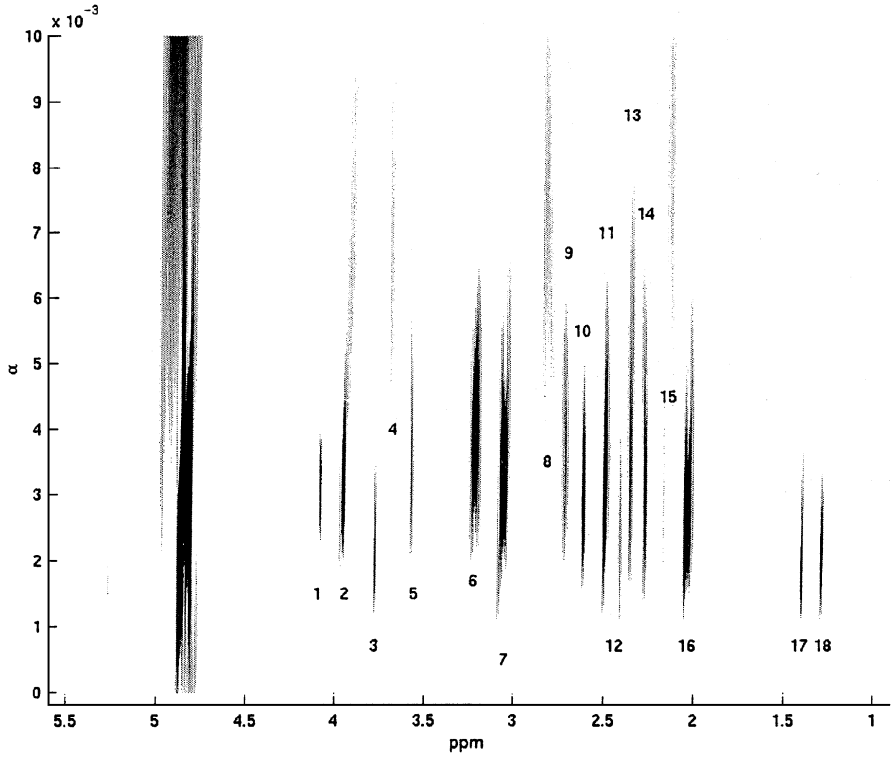

FIG. 11. Top view of the 2D CAPON energy spectrum ($M = 950$) obtained from a standard GE spectroscopic phantom. The phantom contains 12.5 mM NAA, 10.0 mM Cr, 3.0 mM Ch, 7.5 mM mI, 12.5 mM Glu (L-glutamic acid), 5 mM lactate, and 0.5 mM GABA. The signal was acquired on a 1.5-T GE Signa scanner using a PRESS sequence (TE/TR = 144/1500 ms) preceded by CHESS water suppression (voxel size 8 cc). The peaks identified by numbers correspond to the following: 1,5, *myo*-inositol; 2,7, creatine; 3,4, 12–15, glutamate; 6, choline; 8–11, 16, NAA; and 17,18, lactate.

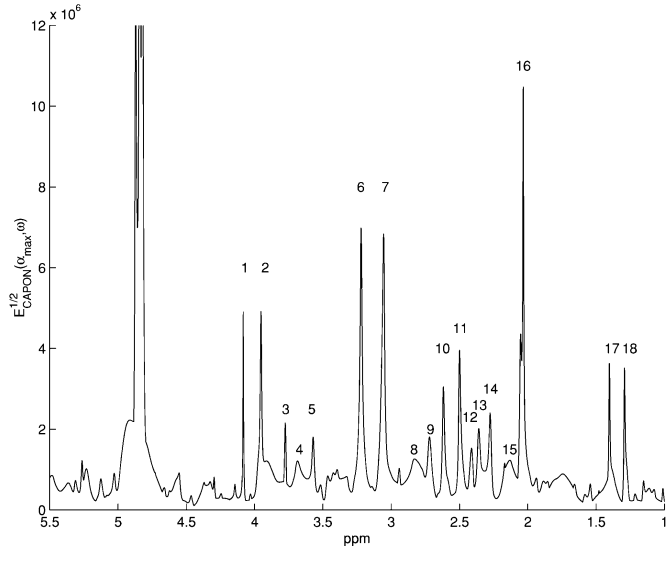

FIG. 12. 1D frequency domain view of the 2D CAPON energy spectrum ($M = 950$) obtained from a standard GE spectroscopic phantom. The phantom contains 12.5 mM NAA, 10.0 mM Cr, 3.0 mM Ch, 7.5 mM mI, 12.5 mM Glu (L-glutamic acid), 5 mM lactate, and 0.5 mM GABA. The signal was acquired on a 1.5-T GE Signa scanner using a PRESS sequence (TE/TR = 144/1500 ms) preceded by CHESS water suppression (voxel size 8 cc). The peaks identified by numbers correspond to the following: 1,5, *myo*-inositol; 2,7, creatine; 3,4, 12–15, glutamate; 6, choline, 8–11, 16, NAA; and 17,18, lactate.

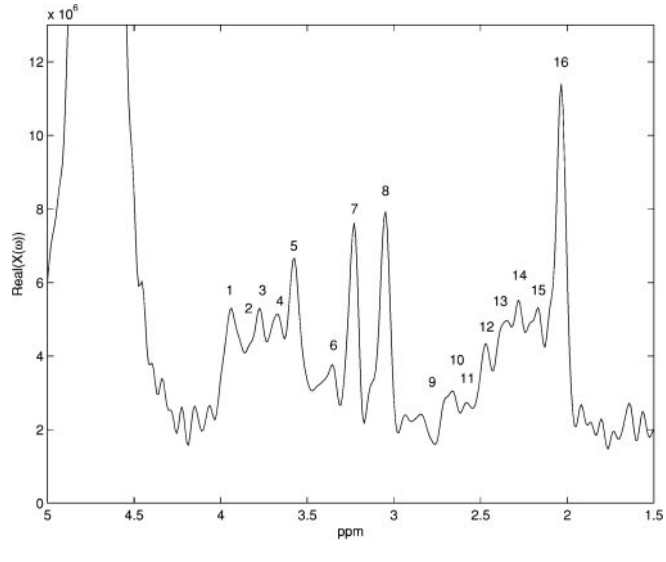

FIG. 13. Phase-corrected 1D FT spectrum from the anterior cingulate gyrus of a 29-year-old healthy male subject. The signal was acquired on a 1.5-T GE Signa scanner using a PRESS sequence (TE/TR = 35/2000 ms) preceded by CHESS water suppression. The spectral bandwidth was 2500 Hz; 2048 points were sampled for each readout, the voxel size is 6 cc, and the total acquisition time is 2 min 40 s. The peaks identified by numbers correspond to the following: 1,8, creatine; 2–4, 13–15, glutamate; 5, *myo*-inositol; 7, choline; and 9–12, 16, NAA.

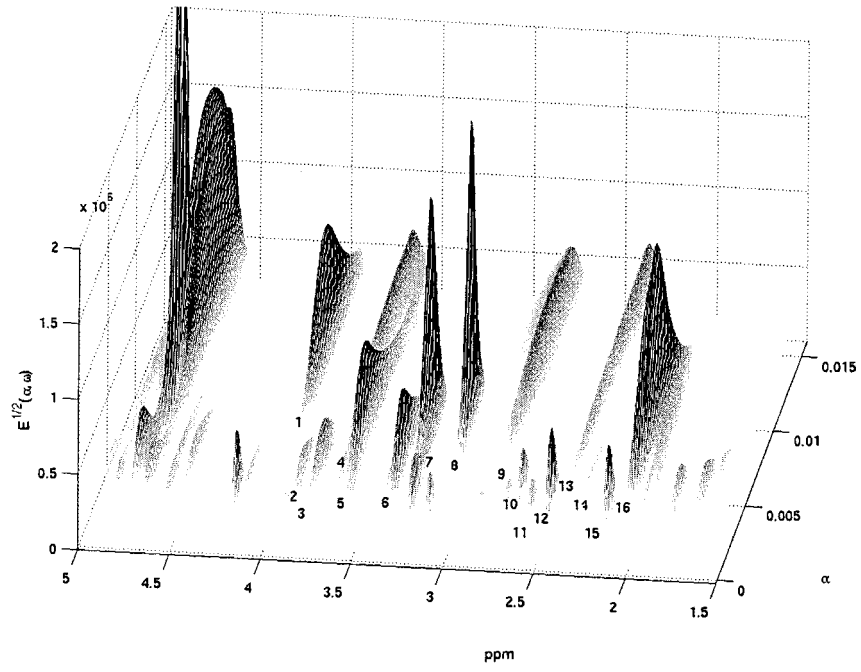

FIG. 14. 2D CAPON energy spectrum ($M = 1000$) from the anterior cingulate gyrus of a 29-year-old healthy male subject. The signal was acquired on a 1.5-T GE Signa scanner using a PRESS sequence (TE/TR = 35/2000 ms) preceded by CHESS water suppression. The spectral bandwidth was 2500 Hz; 2048 points were sampled for each readout, the voxel size is 6 cc, and the total acquisition time is 2 min 40 s. The peaks identified by numbers correspond to the following: 1,8, creatine; 2–4, 13–15, glutamate; 5, *myo*-inositol; 7, choline; and 9–12, 16, NAA.

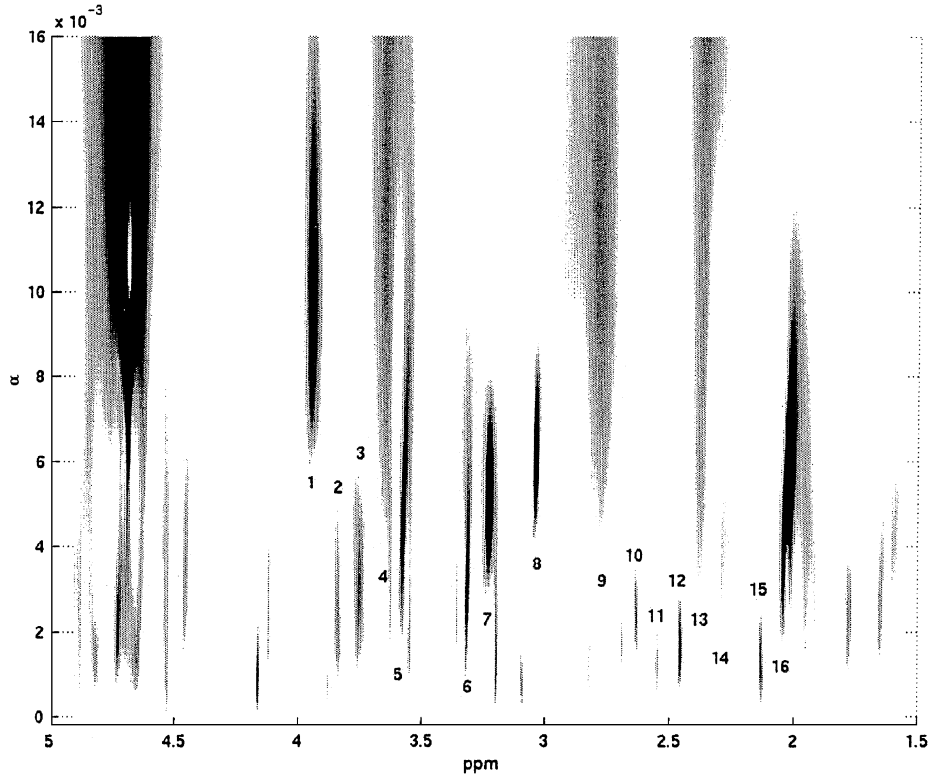

FIG. 15. Top view of the 2D CAPON energy spectrum ($M = 1000$) from the anterior cingulate gyrus of a 29-year-old healthy male subject. The signal was acquired on a 1.5-T GE Signa scanner using a PRESS sequence (TE/TR = 35/2000 ms) preceded by CHESS water suppression. The spectral bandwidth was 2500 Hz; 2048 points were sampled for each readout, the voxel size is 6 cc, and the total acquisition time is 2 min 40 s. The peaks identified by numbers correspond to the following: 1,8, creatine; 2–4, 13–15, glutamate; 5, *myo*-inositol; 7, choline; and 9–12, 16, NAA.

TABLE 1
CAPON and CAPES Amplitude Estimates for the Main Peaks of the GE Spectroscopic Phantom Spectrum Displayed in Fig. 10

		CAPON		CAPES		Expected ratio (TE = 0)
Peak	Substance	$\hat{a}_k$	$\hat{a}_k/\hat{a}_7$	$\hat{a}_k$	$\hat{a}_k/\hat{a}_7$	a_k/a_7
16	NAA	1.55×10^6	1.05	3.92×10^6	1.29	1.3
7	Creatine	1.47×10^6	1	3.03×10^6	1	1
6	Choline	1.41×10^6	0.96	2.57×10^6	0.84	0.9

confirm that the CAPES amplitude estimates are likely to be better than the CAPON amplitude estimates as the CAPES amplitude ratio estimates are closer to what could be expected for the spectroscopic phantom data.

Finally we consider a set of *in vivo* data taken from the anterior cingulate gyrus of a 29-year-old healthy male. The signal was acquired on a 1.5-T GE Signa scanner using a PRESS sequence (TE/TR = 35/2000 ms) preceded by CHESS water suppression. Reference data (8 FIDs, two averages each) were acquired without water suppression, while the metabolite data were acquired with CHESS water suppression (32 FIDs, two averages each). The spectral bandwidth was 2500 Hz; $N = 2048$ points were sampled for each readout. The voxel size was 6 cc and total acquisition time was 2 min 40 s. The phase-corrected 1D FT spectrum is plotted in Fig. 13. The peaks identified by numbers correspond to the following: 1,8, creatine; 2–4, 13–15, glutamate; 5, *myo*-inositol; 7, choline; and 9–12, 16, NAA. Note that the spectrum is relatively noisy and that the resolution is quite poor. The resolution was not visually improved using Gaussian filtering (which therefore was omitted from the figures). The 2D CAPON spectrum ($M = 1000$) is plotted in Fig. 14 and the same spectrum seen from above is displayed in Fig. 15. It can be seen that all the identified peaks are resolved and estimates of the frequency and damping parameters can easily be obtained. Note that a filter order close to $N/2$ was used to achieve this high-resolution spectrum. For comparison the 2D CAPON spectrum is also shown as viewed from the frequency axis in Fig. 16. Even though this 1D view of the 2D spectrum shows a better resolution than that of the 1D FT it is clear that the ability to separate the peaks in two dimensions is essential for visualizing the spectrum of such difficult, realistic *in vivo* NMR signals.

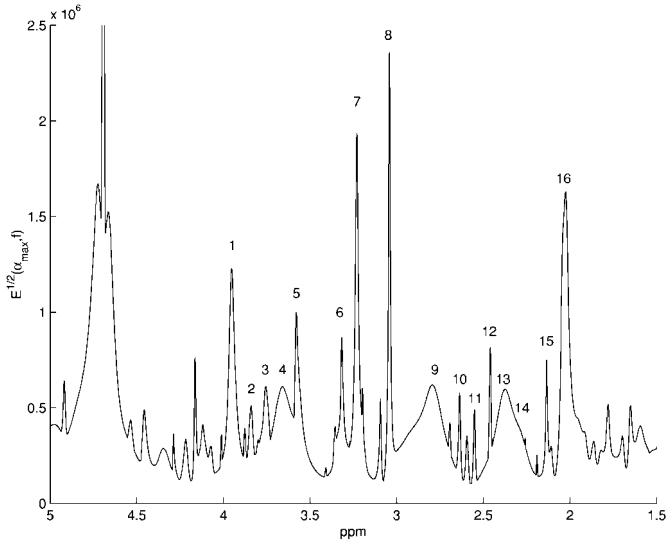

FIG. 16. 1D frequency domain view of the 2D CAPON energy spectrum ($M = 1000$) from the anterior cingulate gyrus of a 29-year-old healthy male subject. The signal was acquired on a 1.5-T GE Signa scanner using a PRESS sequence (TE/TR = 35/2000 ms) preceded by CHESS water suppression. The spectral bandwidth was 2500 Hz; 2048 points were sampled for each readout, the voxel size is 6 cc, and the total acquisition time is 2 min 40 s. The peaks identified by numbers correspond to the following: 1,8, creatine; 2–4, 13–15, glutamate; 5, *myo*-inositol; 7, choline; and 9–12, 16, NAA.

4. CONCLUDING REMARKS

The 2D CAPES method provides a 2D interpretation of NMR spectroscopy data by separating the resonance peaks in both the frequency and the damping domain. The resolution properties are much better than those for the 1D FT even if resolution enhancement techniques such as Gaussian filtering are applied. The 2D spectrum does not require any phasing or baseline correction and does not suffer from any data truncation baseline effects. Furthermore, the choice of its user parameter, M, is much simpler than the choice of the parameters involved with other techniques such as Gaussian filtering. The method is suitable for visualizing most kinds of NMR signals. In particular it can be very useful for low-field NMR spectroscopy where the SNR is low or in cases where there is a strong water signal which severely distorts the 1D FT spectrum.

The parameter estimates obtained by the nonparametric 2D CAPES method are comparable to those obtained by the best parametric methods (such as the NLS). Compared with the latter, 2D CAPES has the significant advantage of being robust to mismodeling. The 2D CAPES method can be used as a standalone estimation method or in combination with some parametric methods. In the latter case 2D CAPES can provide estimates of the frequency and damping parameters that could be used as initial values for the nonlinear search associated with the NLS algorithms.

ACKNOWLEDGMENTS

The authors thank Dr. Elfar Adalsteinsson at the Richard M. Lucas Center for Magnetic Resonance Imaging and Spectroscopy, Stanford University, for providing the spectroscopic phantom data sets as well as giving advice and comments about the "Numerical Examples" section. Furthermore the authors thank Dr. Adolf Pfefferbaum, Director of the Neuropsychiatry Program at SRI International, Menlo Park, for providing the *in vivo* data sets.

REFERENCES

1. J. W. C. van der Veen, R. de Beer, P. R. Luyten, and D. van Ormondt, Accurate quantification of *in vivo* ^{31}P NMR signals using the variable projection method and prior knowledge, *Magn. Reson. Med.* **6,** 92–98 (1988).
2. L. Vanhamme, A. van den Boogaart, and S. Van Huffel, Improved method for accurate and efficient quantification of MRS data with use of prior knowledge, *J. Magn. Reson.* **129,** 35–43 (1997).
3. D. Spielman, P. Webb, and A. Macovski, A statistical framework for *in vivo* spectroscopic imaging, *J. Magn. Reson.* **79,** 66–77 (1988).
4. P. Stoica and T. Sundin, Exact ML-estimation of spectroscopic parameters, *J. Magn. Reson.* **145,** 108–114 (2000).
5. H. Barkhuysen, R. de Beer, W. M. M. J. Bovée, and D. van Ormondt, Retrieval of frequencies, amplitudes, damping factors, and phases from time-domain signals using a linear least-squares procedure, *J. Magn. Reson.* **61,** 465–481 (1985).
6. H. Barkhuysen, R. de Beer, and D. van Ormondt, Improvd algorithm for noniterative time-domain model function to exponentially damped magnetic resonance signals, *J. Magn. Reson.* **73,** 553–557 (1987).
7. Y. Hua and T. K. Sarkar, Matrix pencil method for estimating parameters of exponentially damped/undamped sinusoids in noise, *IEEE Trans. ASSP* **38**(5), 814–824 (1990).
8. P. Stoica and R. Moses, "Introduction to Spectral Analysis," Prentice Hall, Upper Saddle River, NJ (1997).
9. J. Capon, High resolution frequency wave number spectrum analysis, *Proc. IEEE* **57,** 1408–1418 (1969).
10. J. Li and P. Stoica, Adaptive filtering approach to spectral estimation and SAR imaging, *IEEE Trans. Signal Process.* **44**(6), 1469–1484 (1996).
11. P. Stoica, H. Li, and J. Li, A new derivation of the APES filter, *IEEE Signal Process. Lett.* **6**(8), 205–206 (1999).
12. E. G. Larsson and P. Stoica, Fast implementation of two-dimensional APES and CAPON spectral estimators, *Multidimens. Systems Signal Process.*, to appear (2001).
13. A. Jakobsson and P. Stoica, Combining Capon and APES for estimation of spectral lines, *Circuits Systems Signal Process.* **19**(2), 159–169 (2000).
14. P. A. Bottomley, Spatial localization in NMR spectroscopy in vivo, *Ann. N.Y. Acad. Sci.* **508,** 333–348 (1987).
15. A. Haase, J. Frahm, W. Hanicke, and D. Matthaei, 1H NMR chemical shift selective (CHESS) imaging, *Phys. Med. Biol.* **30,** 341–344 (1985).
16. P. G. Webb, N. Sailasuta, S. J. Kohler, T. Raidy, R. A. Moats, and R. E. Hurd, Automated single-voxel proton MRS: Technical development and multisite verification, *Magn. Reson. Med.* **31,** 365–373 (1994).
17. U. Klose, In vivo proton spectroscopy in the presence of eddy currents, *Magn. Reson. Med.* **14,** 26–36 (1990).
18. G. A. Morris, Compensation of instrumental imperfections by deconvolution using an internal reference signal, *J. Magn. Reson.* **80,** 547–552 (1988).